Journal of Magnetism and Magnetic Materials 400 (2016) 107–111

Contents lists available at ScienceDirect

Journal of Magnetism and Magnetic Materials

journal homepage: www.elsevier.com/locate/jmmm

Dynamical vertex approximation for the two-dimensional Hubbard model

Thomas Schäfer, Alessandro Toschi, Karsten Held

Institute for Solid State Physics, TU Wien, 1040 Vienna, Austria

ARTICLE INFO

Article history:
Received 18 June 2015
Received in revised form
23 July 2015
Accepted 28 July 2015
Available online 29 July 2015

Keywords:
Strongly correlated electron systems
Mott–Hubbard transition

ABSTRACT

Recently, diagrammatic extensions of dynamical mean field theory (DMFT) have been proposed for including short- and long-range correlations beyond DMFT on an equal footing. We employ one of these, the dynamical vertex approximation (DΓA), and study the two-dimensional Hubbard model on a square lattice. We define two transition lines in the phase diagram which correspond, respectively, to the opening of the gap in the nodal direction and throughout the Fermi surface. Our self-energy data show that the evolution between the two regimes occurs in a gradual way (crossover) and also that at low enough temperatures the whole Fermi surface is always gapped. Furthermore, we present a comparison of our DΓA calculations at a parameter set where data obtained by other techniques are available.

© 2015 Elsevier B.V. All rights reserved.

1. Introduction

Dynamical mean field theory (DMFT) [1–4] has been a big step forward for the calculation and understanding of strongly correlated electron systems. It includes a major part of the electronic correlations: the local ones. In the vicinity of phase transitions or in one- or two dimensions non-local correlations are however essential. To include non-local correlations but to keep the local DMFT correlations at the same time, cluster extensions of DMFT have been developed such as the dynamical cluster approximation (DCA) [5,6] and cluster DMFT [7,6]. However numerical restrictions regarding the size of the clusters only allow us to treat short range correlations this way. Also the $1/d$ approach [8], a first diagrammatic extension of DMFT by all diagrams occurring in $1/d$ (d: dimension), is restricted to short-ranged correlations.

Hence, as an alternative and to deal with short- and long-range correlations on the same footing, diagrammatic vertex extensions of DMFT have been proposed more recently. The first such approach has been the dynamical vertex approximation (DΓA) [9], followed by the dual fermion (DF) approach [10], the one-particle irreducible approach (1PI) [11], and the merger of DMFT with the functional renormalization group (DMF^{2}RG) [12]. All of these approaches start with a local two-particle vertex [13,14] and calculate from these non-local correlations beyond DMFT. This way, non-local correlations and associated physics are obtained, both, on the two-particle level e.g. for the susceptibilities and on the one-particle-level e.g. for the momentum-dependence of the self-energy. The difference between the various approaches lies in which two-particle vertex is taken: the fully irreducible one (full DΓA), the irreducible one in a certain channel (ladder DΓA), the one-particle irreducible (1PI and DMF^{2}RG) or the reducible one (DF). Then, depending on the approach, Feynman diagrams are constructed from the full Green function G or from the difference between G and the local Green function G_{loc}; and different kind of diagrams are taken: parquet, ladder, 2nd order or the ones generated by an RG flow.

Hitherto, the diagrammatic extensions of DMFT have been applied to simple models, in particular the one-band Hubbard model, though the concept of ab initio calculations with DΓA has also been proposed [15]. Physical highlights so-far have been the calculation of the critical exponents of the three-dimensional Hubbard model [17,18] and the Falicov–Kimball model [19], quantum criticality [20], pseudogaps physics [21,22], and superconductivity [23]. It was also possible to show that the paramagnetic phase of the square lattice Hubbard model is always insulating at low enough temperatures T [24], i.e. that the whole metallic side of the Mott–Hubbard metal-to-insulator transition as described by DMFT is completely washed out by extended long-range spin fluctuations in 2D.

In this paper we recapitulate the DΓA method in Section 2; for further details the reader is referred to [14,25]. Results for the two-dimensional Hubbard model are presented in Section 3. Beyond [24], we analyze further aspects of the transition from the high-T paramagnetic metallic phase to the low-T paramagnetic insulator. In particular, we start by identifying two crossover lines in the phase diagram: first the self-energy at the antinodal momentum $\mathbf{k} = (\pi, 0)$ turns insulating; at a lower T also nodal momentum $\mathbf{k} = (\pi/2, \pi/2)$ shows an insulating behavior. Specifically, our self-energy data demonstrates that the evolution between the two

E-mail address: held@ifp.tuWIEN.ac.at (K. Held).

http://dx.doi.org/10.1016/j.jmmm.2015.07.103
0304-8853/© 2015 Elsevier B.V. All rights reserved.

regimes takes place *gradually* upon decreasing T for all Coulomb interactions U analyzed. In Section 4, we also present, as a benchmark, the comparison of DΓA with DF and DCA. Section 5 summarizes our results.

2. Dynamical vertex approximation

The idea of DΓA is a resummation of Feynman diagrams in terms of the locality of the diagrams, not in orders of U. The first, one-particle level of this resummation is DMFT, which approximates the self-energy, which is the one-particle fully irreducible vertex, to be local. Here, irreducible means that cutting one Green function line does not separate any self-energy diagram into two pieces. Such reducible contributions are then generated by the Dyson equation:

$$G(\nu, \mathbf{k}) = [1/G_0(\nu, \mathbf{k}) - \Sigma(\nu, \mathbf{k})]^{-1}, \tag{1}$$

connecting the Green function $G(\nu, \mathbf{k})$ at Matsubara frequency ν and momentum k (double blue line in Fig. 1), its non-interacting counterpart $G_0(\nu, \mathbf{k}) = 1/[\nu + \mu - \epsilon_k]$ (single blue line) and the self-energy $\Sigma(\nu, \mathbf{k})$ (red circles).

The next, two-particle level then assumes the two-particle fully irreducible vertex to be local. This two-particle level of DΓA is employed nowadays. Before we discuss this approach in further detail, let us mention that, in principle, the fully irreducible n-particle vertex can be assumed to be local. This way more and more contributions are generated, and for $n \to \infty$ the exact solution is recovered. However with increasing n the numerical effort also explodes, and going beyond $n=2$, or possibly $n=3$, does not seem to be feasible.

Let us hence now focus on the two-particle level. The full two-particle vertex F consists of all connected diagrams. Some of these diagrams are two-particle fully irreducible, i.e., cutting two Green function lines G does not separate the diagram into two pieces. We denote these fully irreducible diagrams by Λ. Other (reducible) diagrams separate into two pieces. (Here and in the following we consider skeleton diagrams, i.e., Feynman diagrams in terms of the interacting Green function G instead of those in terms of G_0.)

The *reducible diagrams* of F can be further classified. If we cut two G lines, there are three ways how F separates into two pieces: particle–hole (Φ_{ph}), particle–hole transversal ($\Phi_{\overline{ph}}$) and particle–particle (Φ_{pp}) reducible diagrams, see Fig. 2. One can prove, using particle-conservation, that each diagram is actually either fully irreducible or reducible in *exactly* one channel, so that

$$F(1234) = \Lambda(1234) + \Phi_{ph}(1234) + \Phi_{\overline{ph}}(1234) + \Phi_{pp}(1234). \tag{2}$$

Here, we have introduced a short-hand notation: Eq. (1) represents a momentum-frequency-spin coordinate $1 \equiv (\mathbf{k}, \nu, \sigma)$, $2 \equiv (\mathbf{k}+\mathbf{q}, \nu+\omega, \sigma)$, $3 \equiv (\mathbf{k}'+\mathbf{q}, \nu'+\omega, \sigma')$, $4 \equiv (\mathbf{k}', \nu', \sigma')$. Eq. (2) is known as the *parquet equation*.

Eq. (2) has, for a given Λ, four unknowns: F and three Φ_r's with $r \in \{ph, \overline{ph}, pp\}$. Next, we hence first define the irreducible diagrams in a certain channel r:

$$\Gamma_r(1234) \equiv F(1234) - \Phi_r(1234). \tag{3}$$

From Γ_r, we can then calculate the reducible diagrams by repeatedly connecting them by two Green functions, i.e., formally $\Phi_r = \Gamma_r GG\Gamma_r + \Gamma_r GG\Gamma_r GG\Gamma_r + \cdots$. Inserting this as a recursion into Eq. (3), yields the *Bethe–Salpeter equations* in the three channels (using Einstein's summation convention), see Fig. 3:

$$F(1234) = \Gamma_{ph}(1234) + F(122'1')G(3'2')G(1'4')\Gamma_{ph}(4'3'34) \tag{4}$$

$$= \Gamma_{\overline{ph}}(1234) + F(2'233')G(2'1')G(3'4')\Gamma_{\overline{ph}}(11'4'4) \tag{5}$$

$$= \Gamma_{pp}(1234) + F(4'22'4)G(2'3')G(1'4')\Gamma_{pp}(13'31'). \tag{6}$$

If we now substitute $\Gamma_r(1234) \equiv F(1234) - \Phi_r(1234)$ in the three Bethe–Salpeter equations, we have four equations [Eqs. (2), (4), (5), (6)], which can be resolved for the four unknowns [F, Φ_{ph}, $\Phi_{\overline{ph}}$, and Φ_{pp}].

There is however one further complication, namely the internal Green function lines G in the Bethe–Salpeter equations. These G's can be calculated from Σ via the Dyson equation (1); and Σ in turn can be calculated exactly from F through the Heisenberg equation of motion (also called the Schwinger–Dyson equation in this context):

$$\Sigma(14) = -U(12'3'1')G(1'4')G(23')G(2'3')F(4'234) + U(1234)G(23) - U(1432)G(23) \tag{7}$$

That is the solution of the exact parquet equations involves six equations [(2), (4), (5), (6), (7), (1)] and six unknowns [F, Φ_{ph}, $\Phi_{\overline{ph}}$, Φ_{pp}, Σ, G]. If the exact Λ were known, this would allow us to calculate the exact vertex F, Σ, and G. If not, we still can do approximations for Λ. The so-called parquet approximation assumes $\Lambda = U$ [26]. In DΓA, we consider all Feynman diagrams for Λ in all orders of U, but only take their local contribution. Let us note that the locality assumption for Λ is much better fulfilled than that for Σ. Even for the two dimensional model considered in this paper. Here, DCA calculations have shown Λ to be essentially $\mathbf{k}$-independent [28] while Σ and F are strongly $\mathbf{k}$-dependent.

So-far we have discussed the full (or parquet) DΓA. Often (also for the half-filled Hubbard model discussed in this paper) spin-fluctuations dominate over charge fluctuations at low energies. In this case, the particle–hole and particle–hole transversal channels dominate over the particle–particle channel. Hence, we can neglect Φ_{pp}. Then, the Φ_{ph} and $\Phi_{\overline{ph}}$ channels decouple, and are even related by crossing-symmetry [14], so that the calculation of the two Bethe–Salpeter equations ((4), (6)) (or even one because of the crossing symmetry with a local Γ_{ph} as a starting point) is sufficient. This ladder-DΓA is numerically much easier and the two channels modulo the double counting can be combined to yield the full vertex in Eq. (2) [14,21].

3. Metal-insulator crossover in the 2D Hubbard model

Let us now turn to the ladder-DΓA results for the half-filled Hubbard model on a square lattice with nearest neighbor hopping t and local Coulomb repulsion U, given by the Hamiltonian

$$H = -t \sum_{\langle ij \rangle \sigma} c^\dagger_{i\sigma} c_{j\sigma} + U \sum_i n_{i\uparrow} n_{i\downarrow}. \tag{8}$$

Here, $c^\dagger_{i\sigma}$ ($c_{i\sigma}$) creates (annihilates) an electron on lattice site i with spin σ, $\langle ij \rangle$ sums each nearest neighbor pair once, and energies are from now on measured in units of the half-bandwidth $D=4t$.

The main physical result of [24] is that the low-temperature paramagnetic phase (above the $T=0$ antiferromagnet) is always insulating for all $U > 0$. In other words, the metal-insulator

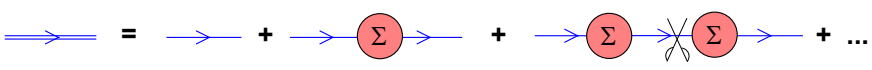


Fig. 1. Graphical representation of the Dyson equation. (For interpretation of the references to color in this figure caption, the reader is referred to the web version of this paper.)

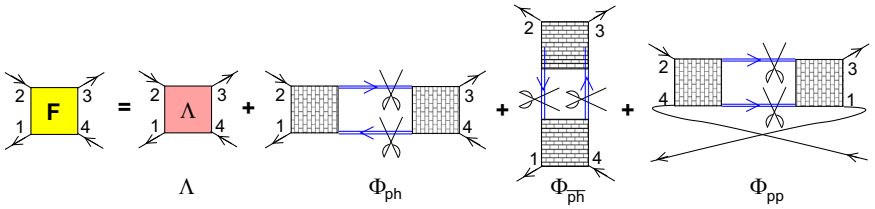


Fig. 2. Graphical representation of the parquet equation: the full vertex F contains fully two-particle irreducible diagrams Λ and two-particle reducible diagrams in the particle–hole Φ_{ph}, transversal particle–hole $\Phi_{\overline{ph}}$, and particle–particle reducible channel Φ_{pp}.

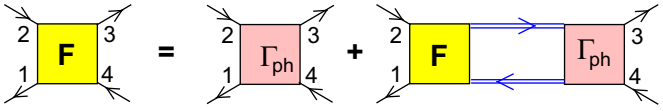


Fig. 3. Bethe–Salpeter equation (4) in the particle–hole (ph) channel.

transition is at $U_c=0$ instead of a finite value $U_c > 0$ which was previously concluded from cluster extensions of DMFT, see, e.g., [27]. As a function of temperature T however, there is a *crossover* from the low-T paramagnetic insulator to a high-T paramagnetic metal at small U's. Here, we analyze in greater detail how this crossover occurs.

Fig. 4 shows the imaginary part of the self-energy for the nodal and antinodal points of the Fermi surface. For $U=0.5$ and high temperatures, $T > 0.017$, the self-energy shows clearly metallic behavior at every point on the Fermi surface from the nodal to the antinodal one. Upon cooling along the gray arrow in Fig. 4, first the antinodal point of the Fermi surface $[k = (\pi, 0)]$ shows a downturn for $\nu \to 0$ in Fig. 4, i.e., an insulating behavior below $T=0.017$.

For $0.017 > T \geq 0.0125$ however, the nodal point of the Fermi surface $[k = (\pi/2, \pi/2)]$ does not show this insulating behavior yet. Only for $T < 0.0125$ this and all other points of the Fermi surface show an insulating self-energy. In other words, for $T < 0.0125$ we have an insulator with the whole Fermi surface gapped, whereas for $0.017 > T \geq 0.0125$ we have a pseudogap with only parts of the Fermi surface gapped.

Hence, upon cooling along the grey arrow in the phase diagram Fig. 5, we hence first cross the dashed red line which marks the temperature where the first point of the Fermi surface $[k = (\pi, 0)]$ shows insulating behavior. At lower temperatures, we cross a second (solid-red) line at which the whole Fermi surface gets gapped. The red-shaded region inbetween hence has a pseudogap.

The analogous analysis for $U=1.0$ can be found in the lower panels of Fig. 4. It corresponds to the second gray arrow in Fig. 5. In this case, we identify a larger pseudogap region at higher temperatures: for $0.05 > T > 0.025$ the nodal self-energy is still metallic whereas the antinodal one is already insulating.

4. Comparison of numerical techniques for the 2D Hubbard model

As mentioned in the Introduction, for the treatment of the two-dimensional Hubbard model there exists a variety of numerical techniques that aim at including correlations beyond the purely temporal but local ones covered by DMFT. Since there is no exact solution of this model in 2D, benchmarks between different methods are of fundamental importance. Fig. 6 shows a self-

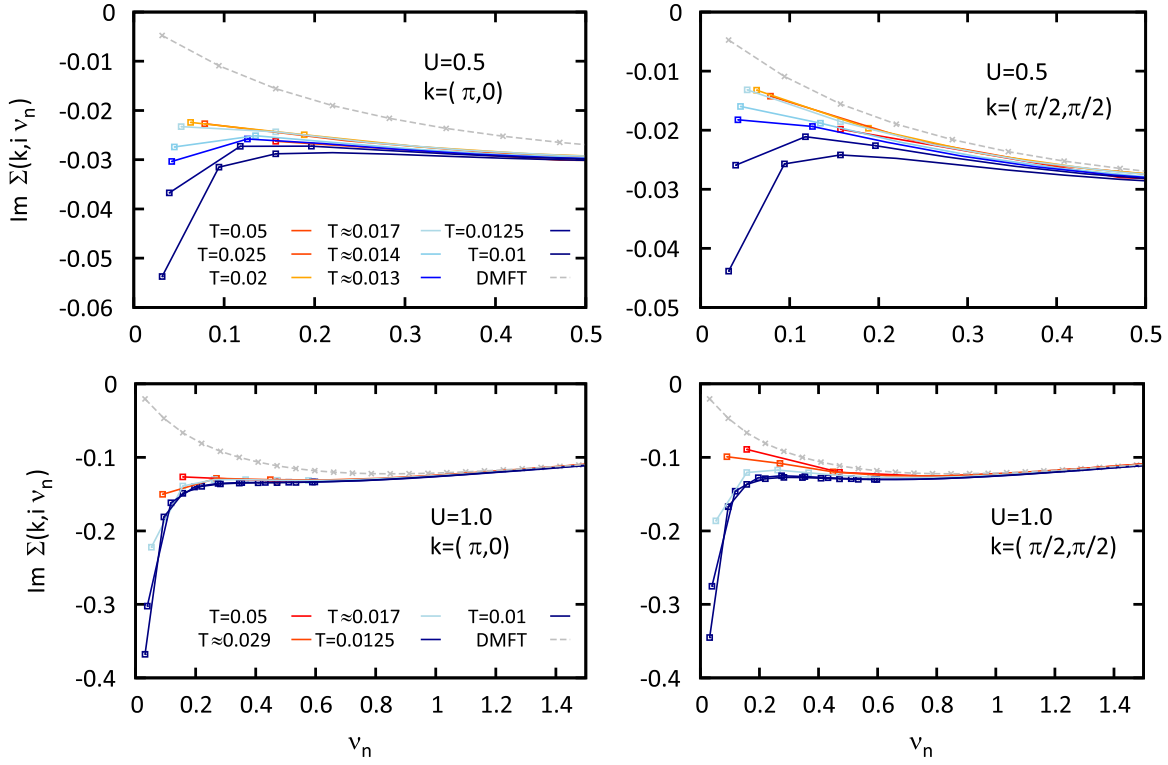


Fig. 4. Imaginary parts of the DΓA self-energy Σ vs Matsubara frequency ν_n for the half-filled Hubbard model at the antinodal (left) and nodal (right) point of the Fermi surface at $U=0.5$ (upper panels) and $U=1.0$ (lower panels) and different temperatures. The DMFT results at $T=0.01$ is provided for comparison.

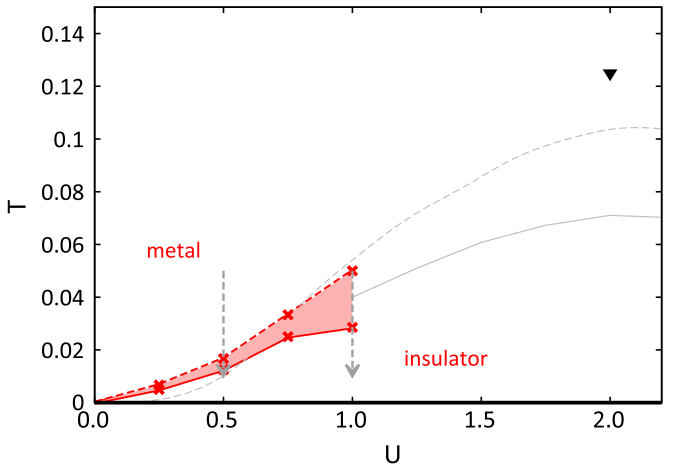


Fig. 5. DΓA phase diagram for the half-filled Hubbard model on a square lattice. Due to strong antiferromagnetic fluctuations, we have a paramagnetic insulator for all $U > 0$ below the solid-red line [24]: upon cooling (e.g. along the vertical arrows that mark the temperatures presented in Fig. 4) first the antinodal point $[k = (\pi, 0)]$ turns insulating at the dashed-red line where the other k points still show a metallic self-energy. That is, in the red-shaded region, we have a crossover with a pseudogap. The dashed-gray and solid-gray line indicates the Néel temperature T_N in DMFT and DΓA for 3D, respectively (for 2D T_N=0 in DΓA). The triangle marks the parameters for the comparison in Fig. 6. (For interpretation of the references to color in this figure caption, the reader is referred to the web version of this paper.)

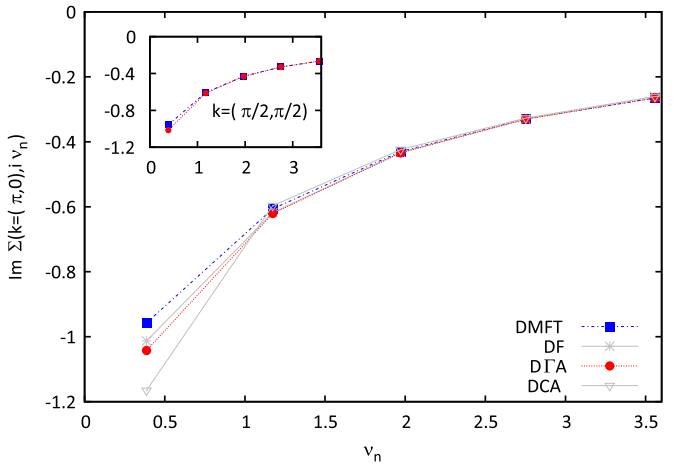


Fig. 6. Comparison of the imaginary parts of DMFT (blue squares), DΓA (red dots), DCA (grey triangles from [29]) and DF (grey stars from [29]) self-energies for the half-filled 2D Hubbard model with U=2.0 and T=0.125. The main plot shows the antinodal point $(k = (\pi, 0))$ and the inset the nodal point $(k = (\pi/2, \pi/2))$ of the Fermi surface. For the latter, no DF/DCA data are available for comparison. (For interpretation of the references to color in this figure caption, the reader is referred to the web version of this paper.)

energy comparison of our DMFT and ladder-DΓA data with the DCA and DF results extracted from the extensive numerical review [29] by LeBlanc et al. for U=2.0 and T=0.125. These parameters correspond to the black triangle in the upper right corner of Fig. 5.

In the main panel of Fig. 6 one can see the data for the antinodal point $k = (\pi, 0)$. Because of the high temperature and large interaction all data sets display an insulating behavior, also DMFT. However, the inclusion of non-local correlations (DCA, DF, DΓA) further enhances the insulating tendencies; the self-energy downturn is more pronounced. The magnitude of this effect is similar in DF and DΓA and somewhat larger in DCA. The overall trend is similar for the nodal point $k = (\pi/2, \pi/2)$ shown as the inset of Fig. 6. In contrast to the weak coupling region which we focused on in Section 3, for this larger U-value we have a Mott–Hubbard insulating behavior for all k points of the Fermi surface. This reflects the increased importance of local correlations in this regime; and even DMFT yields reasonable results.

5. Conclusion

Due to long-ranged antiferromagnetic correlations, the paramagnetic phase of the two-dimensional Hubbard model is insulating at low enough temperatures, half-filling, and a lattice with perfect nesting such as the square lattice with nearest-neighbor hopping — even at an arbitrary small coupling U [24]. For small U and higher temperatures, on the other hand, we have a paramagnetic metal. In this paper, we analyzed the metal-to-insulator crossover in detail. We find that upon cooling, first a gap opens at the antinodal point before, at a lower temperature, the full Fermi surface is gapped. That is, there is a pseudogap. We have also compared our DΓA results with DF and QMC where these are available, i.e., at higher temperatures and intermediate coupling strength. In this parameter regime, DMFT already gives a good description, and all of the three beyond-DMFT approaches show similar corrections to DMFT: non-local correlations systematically increase the insulating tendencies.

Acknowledgments

We thank M. Aichhorn, E. Arrigoni, N. Blümer, F. Geles, E. Gull, A. Katanin, J.P.F. LeBlanc, G. Rohringer, D. Rost, C. Taranto, P. Thunström, J.M. Tomczak, and A. Valli for discussions. Financial support is acknowledged from the Austrian Science Fund (FWF) through graduate school W1243 Solid4Fun (T.S.) and SFB ViCoM (F41, A.T.), as well as from the European Research Council under the European Union's Seventh Framework Programme (FP/2007-2013)/ERC through grant agreement n. 306447 (*AbinitioDΓA*, K.H.). The calculations were performed on the Vienna Scientific Cluster (VSC).

References

[1] W. Metzner, D. Vollhardt, Phys. Rev. Lett. 62 (1989) 324.
[2] A. Georges, G. Kotliar, Phys. Rev. B 45 (1992) 6479.
[3] A. Georges, G. Kotliar, W. Krauth, M. Rozenberg, Rev. Mod. Phys. 68 (1996) 13.
[4] G. Kotliar, D. Vollhardt, Phys. Today 57 (March (3)) (2004) 53.
[5] T. Maier, et al., Rev. Mod. Phys. 77 (2005) 1027.
[6] A.I. Lichtenstein, M.I. Katsnelson, Phys. Rev. B 62 (2000) 9283 , R.
[7] G. Kotliar, et al., Phys. Rev. Lett. 87 (2001) 186401.
[8] A. Schiller, K. Ingersent, Phys. Rev. Lett. 75 (1995) 113;
G. Zaránd, D.L. Cox, A. Schiller, Phys. Rev. B 62 (2000) 16227 , R.
[9] A. Toschi, A.A. Katanin, K. Held, Phys. Rev. B 75 (2007) 045118;
A. Toschi, A.A. Katanin, K. Held, Prog. Theor. Phys. Suppl. 176 (2008) 117.
[10] A.N. Rubtsov, et al., Phys. Rev. B 77 (2008) 033101.
[11] G. Rohringer, et al., Phys. Rev. B 88 (2013) 115112.
[12] C. Taranto, et al., Phys. Rev. Lett. 112 (2014) 196402.
[13] G. Rohringer, et al., Phys. Rev. B 86 (2012) 125114;
T. Schäfer, et al., Phys. Rev. Lett. 110 (2013) 246405.
[14] G. Rohringer, Ph.D. thesis, Vienna University of Technology, 2013.
[15] A. Toschi, et al., Ann. Phys. 523 (2011) 698 , cf. [16].
[16] K. Held et al., Hedin equations, GW, GW+DMFT, and all that, in: E. Pavarini, E. Koch, D. Vollhardt, A. Lichtenstein (Eds.), The LDA+DMFT Approach to Strongly Correlated Materials - Lecture Notes of the Autumn School 2011 Hands-on LDA+DMFT, Reihe Modeling and Simulation, vol. 1, Forschungszentrum Jülich, 2011.
[17] G. Rohringer, et al., Phys. Rev. Lett. 107 (2011) 256402.
[18] D. Hirschmeier et al., arxiv:1507.00616.
[19] A.E. Antipov, et al., Phys. Rev. Lett. 112 (2014) 226401.
[20] T. Schäfer et al. (unpublished).
[21] A.A. Katanin, A. Toschi, K. Held, Phys. Rev. B 80 (2009) 075104.
[22] A.N. Rubtsov, et al., Phys. Rev. B 79 (2009) 045133.
[23] J. Otsuki, et al., Phys. Rev. B 90 (2014) 235132.
[24] T. Schäfer, et al., Phys. Rev. B 91 (2015) 125109.
[25] K. Held, Dynamical vertex approximation, in: E. Pavarini, E. Koch, D.Vollhardt, A. Lichtenstein (Eds.), Autumn School on Correlated Electrons. DMFT at 25:

Infinite Dimensions, Reihe Modeling and Simulation, vol. 4, Forschungszentrum Jülich, 2014 arxiv:1411.5191.
[26] N.E. Bickers, Self consistent many-body theory of condensed matter, in: Theoretical Methods for Strongly Correlated Electrons CRM Series in Mathematical Physics Part III, Springer, New York, 2004.
[27] H. Park, K. Haule, G. Kotliar, Phys. Rev. Lett. 101 (2008) 186403.
[28] T.A. Maier, et al., Phys. Rev. Lett. 96 (2006) 047005.
[29] J.P.F. LeBlanc et al., arXiv:1505.02290, 2015.